Influence of Recycle Operation on the Catalytic Hydrogenation of CO_2 to Long-Chain Hydrocarbons

Lucas Brübach,* Dennis Trützler, Daniel Hodonj, and Peter Pfeifer

ABSTRACT: The catalytic hydrogenation of CO_2 to long-chain hydrocarbons (CO_2-based Fischer−Tropsch synthesis) may become an important industrial process for the production of sustainable hydrocarbons for the chemical industry or fuel applications in the future. Several questions regarding the scale-up of the process remain unsolved, though, as there have scarcely been studies beyond lab-scale. Recycle operation might be necessary in a technical application to achieve high reactant conversions. However, as not only unconverted reactants but also light hydrocarbons are recycled into the reactor, the product composition might be significantly altered. In this study, we investigated the influence of recycle operation in a bench scale recycle reactor setup (10−20 g catalyst) for a potassium promoted, alumina supported iron catalyst at 300 °C, 10 bar, $(H_2/CO_2)_{in}$ = 3, and fresh feed space velocities ranging from 1800 to 7200 $mL_N\,h^{-1}\,g^{-1}$. An increase in reactant conversion could be clearly observed under recycle conditions which can be well described with previously developed models. The product composition, however, was only slightly affected. The data indicates a slight increase of the average molecular weight under recycle conditions which may be caused not only by secondary reactions of linear 1-alkenes but also by more favorable synthesis conditions. Among secondary reactions of linear 1-alkenes, there was only convincing evidence for hydrogenation (especially for ethene) and double-bond-shift.

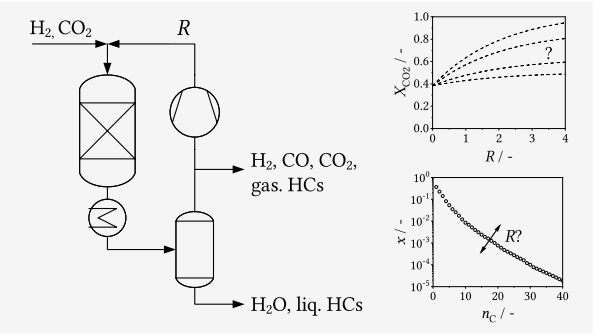

1. INTRODUCTION

The catalytic hydrogenation of CO_2 to long-chain hydrocarbons is a highly promising process for the production of sustainable hydrocarbons. Currently, it is extensively investigated worldwide as a future source for basic chemicals or fuel applications.[1−6] One possible pathway is the CO_2-based Fischer−Tropsch synthesis (CO_2−FTS) which is essentially a combination of the reverse water gas shift (RWGS) and subsequent FTS in one reactor. Alkali promoted, iron based catalysts are usually applied for this process as they catalyze both reactions.[4] The overall reaction is given by eq 1.

$$n\mathrm{CO_2} + 3n\mathrm{H_2} \rightarrow (\mathrm{CH_2})_n + 2n\mathrm{H_2O} \quad (1)$$

For the scale-up of the CO_2−FTS, water removal is a key step to achieve high reactant conversions.[7] Water is the main product and does not only strongly inhibit the reaction[7,8] but may also lead to catalyst degradation via oxidation at high water partial pressures.[8,10] Rohde et al.[11] proposed and tested a membrane reactor to achieve an in situ removal of the formed water. However, such membrane concepts require further development for an industrial application.[12] Currently, condensation appears to be the only reasonable technical solution. This leads to two process concepts that have already been proposed in a patent from 1954:[13] multiple reactors in series with intermediate condensation or a recycle reactor with continuous condensation.

Very few experimental studies of these two concepts have been performed, so far. Two reactors in series have been studied by Guo et al.[14] and Lee et al.[15] who could demonstrate the anticipated increase in reactant conversion. Landau et al.[8] demonstrated a CO_2 conversion of up to 89% utilizing 3 reactors in series. Choi et al.[16] and Lee et al.[15] published results under recycle conditions. Unfortunately, they provided only very few details of their results. Recently, Willauer et al.[17] reported on a fixed-bed reactor prototype which allowed for a significant increase of CO_2 conversion under recycle conditions.

Additionally to the increase in reactant consumption, possible secondary reactions of recycled hydrocarbons are highly important for further process development steps as they will affect the product composition. The influence and extent

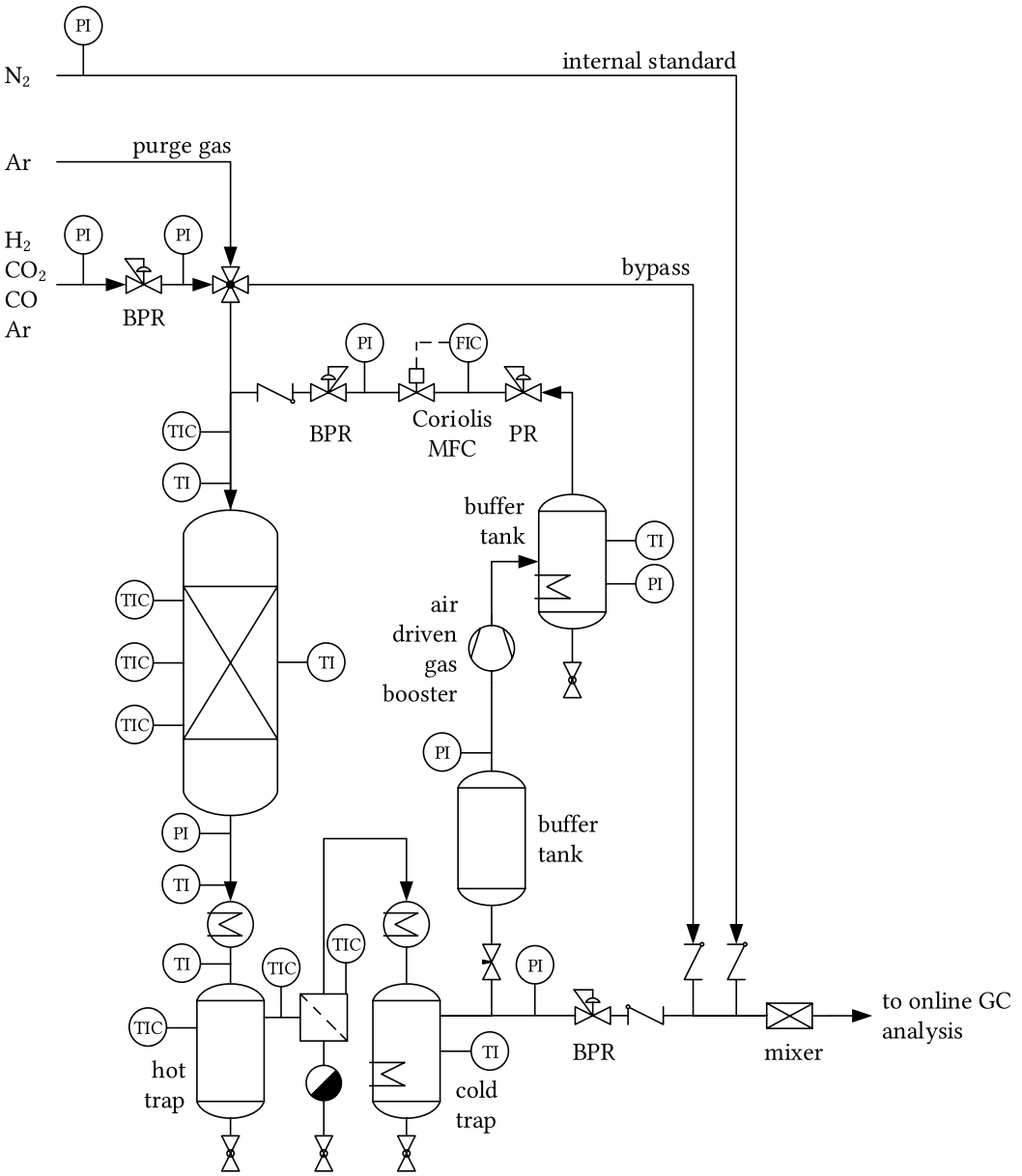

Figure 1. Simplified flow scheme of the bench scale recycle reactor setup (FIC: flow indicator controller, PI: pressure indicator, TI: temperature indicator, TIC: temperature indicator controller, PR: pressure regulator, BPR: back pressure regulator, MFC: mass flow controller, GC: gas chromatograph).

of secondary reactions of 1-alkenes has been a controversial topic in conventional Fischer–Tropsch research for decades and is still under debate.[18] Here, only studies of iron-based catalysts will be considered, as the mechanisms for cobalt might differ significantly. The following secondary reactions of 1-alkenes were reported for the traditional iron-FTS: hydrogenation,[19−23] isomerization (double-bond-shift),[19,21] reincorporation/secondary growth,[19,21−23] hydrogenolysis,[19,23] and carbonylation.[22] Among the secondary reactions, ethene hydrogenation seems to be the most relevant one under industrial conditions.[20]

It was pointed out by Boelee et al. that the 1-alkene/CO ratio has a strong influence on the extent of secondary reactions as they would compete for the same catalyst sites.[24] Considering the fact that the CO partial pressure is very low under CO_2–FTS conditions, secondary reactions may be more relevant than in the conventional FTS. On the contrary, potassium promotion (which is very common for CO_2–FTS catalysts[4]) is reported to suppress secondary reactions.[25]

In this study, the influence of recycle operation on reactant consumption and product distribution was investigated for the catalytic hydrogenation of CO_2 to long-chain hydrocarbons (CO_2–FTS). The experiments were conducted in a bench scale fixed bed recycle reactor setup with an in-house prepared supported iron catalyst. Prior to the recycle experiments, different sieve fractions of the catalyst were tested at lab-scale to assess the catalytic performance.

2. EXPERIMENTAL SECTION

2.1. Catalyst Preparation and Characterization. In our previous work, an alumina supported iron catalyst (Fe–K/γ-Al_2O_3) was prepared with a two step incipient wetness impregnation of γ-Al_2O_3 particles (100–200 μm crushed extrudates - Sasol Alumina Extrudates 1.5/150 TH 100).[9]

The support was impregnated with an aqueous solution of $Fe(NO_3)_3 \cdot 9H_2O$ (Merck Supelco Emsure), dried, and calcined. Then, the steps were repeated with an aqueous solution of K_2CO_3 (Alfa Aesar). Overall, it was aimed for a nominal metal loading of 15 and 5.25 wt % (on support weight basis) of Fe and K, respectively. This catalyst will be referred to as Fe−K/γ-Al_2O_3−I.

For the bench scale setup, larger particles were required to reduce the pressure drop of the catalyst bed. Thus, whole 1.5 mm extrudates (Sasol Alumina Extrudates 1.5/150 TH 100) were impregnated. When applying the exact same impregnation procedure as for the powder, it was not possible to achieve a uniform iron distribution along the extrudate radius. The first step was thus switched to a wet impregnation: The extrudates were completely soaked into a $Fe(NO_3)_3$ solution for 16 h at 40 °C. During this time the solution was gently stirred. The exact recipe is given in the Supporting Information. This catalyst will be referred to as Fe−K/γ-Al_2O_3−II. The wet impregnation did not allow for a precise control of the metal loading. This problem will be discussed in Section 4.1.

The catalysts (Fe−K/γ-Al_2O_3−I and Fe−K/γ-Al_2O_3−II) were characterized via N_2 physisorption, Hg porosimetry, and inductively coupled plasma optical emission spectrometry (ICP-OES). To compare the catalytic activity, both catalysts were investigated in a 300 h time-on-stream (TOS) run. To check for a possible intraparticle diffusion limitation, 4 different sieve fractions (50−100 μm, 100−200 μm, 300−400 μm, 500−1000 μm) of crushed Fe−K/γ-Al_2O_3−II extrudates were tested under the same conditions. Larger particles could not be tested under these conditions without the risk of wall effects due to the applied reactor diameter. For the recycle experiments, the 500−1000 μm sieve fraction of Fe−K/γ-Al_2O_3−II was used which was found to be most suitable from a practical point of view (low pressure drop, negligible wall effects, and simple handling).

2.2. Experimental Setups. The long-term catalytic activity, as well as particle size variation tests, were performed in a lab-scale setup that has been previously presented.[9] The long-term tests were conducted with 2 g catalyst (100−200 μm), diluted with 2 g of SiC (ESK-SIC GmbH, 200−300 μm), and the particle size variation tests were conducted with 1 g catalyst, diluted with 12 g of SiC (200−300 μm). Different from the original publication, we used a 1/2″ stainless steel tube with an inner diameter of 10.9 mm for the particle size variation tests to avoid wall effects.

The focus of this work is recycle experiments which were performed in a newly erected recycle reactor setup. A simplified flow scheme of the setup is given in Figure 1. The gases (H_2, CO_2, CO, Ar, N_2) were dosed with mass flow controllers (MFC, Brooks SLA 5850) with up- and downstream pressures being regulated to ensure calibration conditions at all times. All gases were supplied by Air Liquide (purity: H_2, Ar, N_2>99.999%; CO_2>99.995%; CO >99.97%).

The reactor consisted of a 365 mm long stainless steel tube (ID: 20 mm, OD: 30 mm) with 1″ VCR fittings (Swagelok). The reactor temperature was controlled with 3 separately heated brass jackets (250 W), each being 95 mm long with a 5 mm distance between each other. The temperature in the catalyst bed was measured with an axially moveable thermocouple (type K) that was led through a centrally positioned 3 mm OD stainless steel tube or a multipoint thermocouple (OD: 3 mm, type K, 7 points) that was centrally fixed inside the reactor. For the experiments, a 20 cm long catalyst bed was used which was positioned in the middle of the reactor. The fixed bed consisted of 10 or 20 g catalyst diluted with 90 or 64 g silicon carbide particles (ESK-SIC GmbH, grit F24, ≈500−1000 μm). The remaining space above and below the catalyst bed was filled with silicon carbide particles (grit F24).

The product gas was cooled down in a microstructured heat exchanger and subsequently led through a hot trap (140 °C, 1 L) to separate the wax fraction. The separation of wax droplets from the gas stream proved to be a major challenge. Thus, we installed a heated (140 °C) coalescence filter with a drainage sump (Infiltec GmbH) after the hot trap. Without the filter, we encountered serious pressure fluctuations in the setup due to wax deposits. After the filter, the product stream was cooled down further with a second microstructured heat exchanger, and the liquid phases (oil and water) were collected in a cold trap (5−10 °C, 3.8 L). The remaining gas left the setup through a back pressure regulator (Equilibar LF Research Series) and was mixed with the internal standard (N_2) for the online GC analysis.

A key feature of the setup was an air driven gas booster (Maximator DLE 5-2) which allowed the partial recycling of product gas. Buffer tanks were installed at the inlet (volume: 1 L) and outlet (volume: ≈0.5 L) of the compressor to avoid pressure fluctuations in the main part of the setup. Additionally, the buffer tank at the outlet allowed for the separation and draining of condensate. Condensate formation was usually not observed, though. The recycle mass flow rate was controlled with a Coriolis MFC (Bronkhorst mini CORI-FLOW M13 V10l) to ensure a precise flow control, independent from the gas composition. Again, up- and downstream pressures of the MFC were regulated to improve the stability of the flow control.

The system pressures and temperatures were measured at several positions using electronic pressure transmitters (WIKA S-20) and thermocouples (type K). The whole setup was monitored and controlled with a cRIO-9056 controller (National Instruments).

2.3. Data Analysis and Definitions. The gas hourly space velocity ($GHSV_F$) is defined as the ratio of the volumetric feed flow rate ($\dot{V}$) at normal conditions (subscript N, 0 °C, and 1 atm) with respect to the catalyst mass (m_{cat}). It is important to highlight that $GHSV_F$ was always related to the fresh feed flow rate, independent of a possible gas recycle.

$$GHSV_F = \frac{\dot{V}_{F,N}}{m_{cat}} \tag{2}$$

The recycle ratio (R) is defined as the ratio of the mass flow of recycled gas ($\dot{m}_R$) to the fresh feed mass flow rate ($\dot{m}_F$).

$$R = \frac{\dot{m}_R}{\dot{m}_F} \tag{3}$$

The conversion of CO_2 and H_2 is calculated as either the overall conversion of the whole setup (X_i) or conversion per reactor pass. It is calculated from the molar flow rates at the inlet ($\dot{n}_{i,in}$) and outlet ($\dot{n}_{i,out}$) of the corresponding system boundaries.

$$X_i = \frac{\dot{n}_{i,in} - \dot{n}_{i,out}}{\dot{n}_{i,in}} \tag{4}$$

The overall selectivity to CO (S_{CO}) is calculated from the molar flow rate of formed CO with respect to the overall converted amount of CO_2. The selectivity to CO per reactor pass is not addressed. It is always given with respect to the whole setup.

$$S_{CO} = \frac{\dot{n}_{CO,out}}{\dot{n}_{CO_2,in} - \dot{n}_{CO_2,out}} \quad (5)$$

For the hydrocarbon products, a different selectivity ($S_{i,HC}$) is used which excludes CO. It is calculated on a carbon basis from the molar flow rate of hydrocarbon species i multiplied by its carbon number $n_{i,C}$. It is more reasonable to use this measure when comparing hydrocarbon selectivities of different experiments as it is not biased by the CO selectivity. This measure is sometimes referred to as "CO-free" selectivity. Again, selectivities per pass are not considered.

$$S_{i,HC} = \frac{\dot{n}_{i,out} n_{i,C}}{\dot{n}_{CO_2,in} - \dot{n}_{CO_2,out} - \dot{n}_{CO,out}} \quad (6)$$

2.4. Experimental Procedures. For the catalyst activation, we adapted a combined reduction/carburization method that had been originally proposed by Landau et al.[26] The catalyst was first reduced under pure H_2 at 450 °C for 16 h at a flow rate of 100 $mL_N\ min^{-1}\ g_{cat}^{-1}$ and afterward carburized with diluted syngas (molar ratio $H_2/CO/Ar$: 1/1/2) at a flow rate of 200 $mL_N\ min^{-1}\ g_{cat}^{-1}$ for 5 h. The experimental conditions of the catalyst tests in the lab-scale setup are given in Table 1. For these experiments, isothermal conditions (set-point ± 1 K in radial and axial direction) could be assured in the catalyst bed.

Table 1. Experimental Conditions for Long Term Catalytic Activity and Particle Size Variation Tests in the Lab-Scale Setup[a]

catalyst	mass (g)	sieve fraction (μm)	T (°C)	$GHSV_F$ ($mL_N\ h^{-1}\ g^{-1}$)	TOS (h)
Fe−K/γ-Al_2O_3−I[b]	2	100−200	300	1800	300
Fe−K/γ-Al_2O_3−II	2	100−200	300	1800	300
Fe−K/γ-Al_2O_3−II	1	50−100	320	14400	50
Fe−K/γ-Al_2O_3−II	1	100−200	320	14400	50
Fe−K/γ-Al_2O_3−II	1	300−400	320	14400	50
Fe−K/γ-Al_2O_3−II	1	500−1000	320	14400	50

[a]All runs were conducted at 10 bar and an H_2/CO_2 molar inlet ratio of 3. [b]Detailed results of this run have been previously published.[9]

For the recycle experiments, the same activation procedure was applied. However, we used a significantly higher dilution ratio and flow rate at the beginning of the carburization step (molar ratio $H_2/CO/Ar$: 5/1/50 at an absolute flow rate of 5600 $mL_N\ min^{-1}$). The dilution was reduced stepwise within 12 min to the relative flow rates given above. The freshly reduced catalyst is extremely active upon exposure to CO, and a thermal runaway can occur if no care is applied. When the activation was finished, the setup was pressurized with hydrogen, and the feed was dosed. For the recycle experiments, the reactor was started up in once-through mode and operated like this overnight. This was necessary to flush the system volume with product gas before ramping up the recycle compressor. Within one experimental run, the recycle ratio was then stepwise increased. The reference experiments without a recycle were conducted in a separate run.

The experimental plan of the recycle experiments is given in Table 2. The carbon balance was closed between 96 and 99%

Table 2. Experimental Conditions for the Recycle Experiments[a]

$GHSV_F$($mL_N\ h^{-1}\ g^{-1}$)	m_{cat} (g)	m_{SiC} (g)	R(-)
1800, 3600, 7200	10	90	0
1800	20	64	1, 2, 4, 8[b]
3600	10	90	1, 2, 4, 8[b]
7200	10	90	1, 2, 4[b]

[a]All runs were conducted with Fe−K/γ-Al_2O_3−II (500−1000 μm) at 10 bar, an outer reactor wall temperature of 300 °C, and an H_2/CO_2 molar inlet ratio of 3. [b]Strong and irreversible catalyst deactivation occurred under these conditions; results are excluded from further analysis.

for all experiments (see the Supporting Information for a detailed table). It has to be highlighted again that $GHSV_F$ for the recycle experiments is given with respect to the fresh feed flow rate. The fresh feed flow rate was not adjusted within the recycle experiments. The outer wall temperature (T_W) was kept constant at 300 °C for all experiments. The size of the reactor did not allow for isothermal operation, though. The inner temperature of the catalyst zone ranged from 298 °C to a maximum of 308 °C at the hot spot in the most extreme case. Exemplary temperature profiles are given in the Supporting Information. For the liquid product sampling, the product traps were emptied ≈5 h after a change in process conditions. The liquid products were then collected until the next change of process conditions (1−3 days).

2.5. Product Analysis. For the catalyst tests in the lab-scale setup, we only considered the gas phase analysis via online GC. This was sufficient for the envisaged comparisons here. The configuration of the GC is given below.

The product of the recycle reactor system consisted of four different phases (gas, oil, water, and wax) which had to be quantified and analyzed separately. Quantification of the gas phase was achieved with an internal standard (N_2). The amount of oil, water, and wax was determined via weighing. The determined mass was then divided by the collection time to obtain the mass flow rate. The separation of the oil and water phase was performed manually with a separation funnel.

The gas phase was analyzed online with a customized GC system (Agilent 8890, customized by Teckso GmbH). It comprised 5 valves, 5 columns, and 3 detectors. Permanent gases (H_2, N_2, CO_2, CO, and CH_4) were separated on micropacked columns (HaysepQ and MS5A) and quantified with a TCD. C_1−C_6 hydrocarbons were separated on a GS-GasPro column (Agilent, 30 m, 320 μm ID) and detected with an FID. Long-chain hydrocarbons were separated on an HP-5 column (Agilent, 60 m, 250 μm ID, 0.25 μm film) and detected with a second FID. The quantification of permanent gases was achieved with individual calibrations that were determined in advance using reference gas mixtures (basi Schöberl). Hydrocarbons were quantified using CH_4 as the reference gas and carbon based relative response factors of 1 for all components.

The oil and water phases were analyzed via GC-FID (Agilent 7820A) on an Rtx-1 column (Restek, 60 m, 320 μm ID, 1 μm film) using split injection. A deactivated liner (Topaz precision liner with wool, Restek) was used to minimize adsorption of components in the GC inlet. The oil samples were analyzed without dilution or internal standard. The

quantification was performed with a 100% method and response factors of 1 for all components. For the water samples, dimethoxyethane was used as an internal standard (≈1% by weight). Relative response factors of the analytes were determined in advance with self-prepared calibration mixtures applying a 3-point calibration. We are fully aware that the applied column was a poor choice for the water analysis. The relatively low column capacity led to strong fronting of the carboxylic acid peaks (here: ethanoic and propionic acid). However, we could still achieve a reproducible analysis and considered the analytical quality sufficient for the intended analysis.

The wax phase was analyzed via high-temperature GC-FID (Agilent 7890B) on an MXT-1 column (Restek, 30 m, 530 μm ID, 0.25 μm film). The wax samples were dissolved in *n*-hexane (Supelco SupraSolv, 5 g L^{-1}) and introduced onto the column via direct injection using a programmable temperature inlet (Da Vinci Laboratory Solutions PTI 1.5). As for the oil, the quantification was performed with a 100% method and response factors of 1 for all components.

The product spectrum was extremely complex with several hundred different species (likely more than a thousand) comprising *n*-alkanes, iso-alkanes, cyclo-alkanes, linear alkenes, iso-alkenes, aromatic components, and oxygenates. With the available analytical equipment, it was only possible to assign each species up to C_3. Up to C_{20}, we allocated linear 1-alkenes (referred to as 1-alkenes here) and *n*-alkanes. All other hydrocarbons were lumped into the group *other*. Beyond C_{20}, we only determined the carbon number mass fraction.

3. MODELING

3.1. Reactor Modeling. The recycle reactor was modeled as an isothermal, pseudohomogeneous, and isobaric ideal plug flow reactor (PFR). Due to the rather small temperature gradients in the catalyst bed, we did not solve the heat balance for simplification. We assumed an average temperature of 303 °C for all experiments. The remaining simplifications were considered to be justified based on common criteria ($Bo > 100$, $d_T/d_P > 8$, pressure drop < 10%) and the particle size variation tests (see explicitly section 4.1.2).

3.2. Kinetic Modeling. A simple global kinetic model, as well as a detailed, mechanism-based, kinetic model, was recently published by us for Fe−K/γ-Al_2O_3−I.[9,27] Details about the models are given in the original publications. The simulations of the recycle experiments are based on the detailed, mechanism-based model which allows for the simultaneous prediction of reactant consumption and product distribution. The consideration of the product distribution is especially important when modeling a recycle reactor since also hydrocarbons are recycled which may undergo secondary reactions or act as a diluent.

We have to emphasize that both models were developed for Fe−K/γ-Al_2O_3−I and not Fe−K/γ-Al_2O_3−II. To account for the slightly different activities of the catalysts, we increased the catalyst mass by 20% within the simulations to adapt to the experimentally determined conversion levels of Fe−K/γ-Al_2O_3−II (see section 4.1).

3.3. Phase Equilibria Modeling. For a realistic mathematical representation of the recycle setup, it was further necessary to model the phase equilibria in the product traps in combination with the detailed kinetic model.

We applied the Predictive Soave−Redlich−Kwong (PSRK) equation of state (EOS)[28] which can be expected to yield reliable VLE and VLLE predictions for FT systems.[29,30] PSRK is a group contribution based EOS which combines the Soave−Redlich−Kwong (SRK) EOS[31] with the original UNIFAC model.[32] This combination allows the VLE and VLLE modeling of complex mixtures containing super- and subcritical components. It was not possible to use the more recent successor model, the Volume-Translated Peng−Robinson EOS,[33] due to an insufficient publicly available interaction parameter database.

Details about the PSRK model,[28,34,35] the applied flash algorithms,[36,37] example calculations for reference systems,[38−40] and the pure component data compilation approach (critical property data and Mathias−Copeman parameters[41]) are given in the Supporting Information. The hot trap was modeled with a two-phase flash algorithm (VLE) at 140 °C and the cold trap with a three-phase flash algorithm (VLLE) at 8 °C.

4. RESULTS AND DISCUSSION

4.1. Catalyst Tests. *4.1.1. Influence of Catalyst Preparation.* The key results of the long-term catalytic activity tests of Fe−K/γ-Al_2O_3−I and Fe−K/γ-Al_2O_3−II are given in Table 4. A graphical presentation of the data over TOS is provided in the Supporting Information. Some physical and chemical properties determined via N_2 physisorption and ICP-OES are given in Table 3.

Table 3. Key Properties of the Investigated Catalysts Determined via N_2 Physisorption and ICP-OES

catalyst	BET surface area ($m^2\ g^{-1}$)	Fe loading (wt.-%)	K loading (wt.-%)
Fe−K/γ-Al_2O_3−I	113	15.1 ± 0.8	5.3 ± 0.3
Fe−K/γ-Al_2O_3−II	103	19.3 ± 1.1	6.3 ± 0.4

Table 4. Results of the Long-Term Catalytic Activity Tests[a]

catalyst	TOS (h)	X_{CO_2} (%)	S_{CO} (%)	$S_{CH_4,HC}$ (%)	$S_{C_{5+},HC}$[b] (%)
Fe−K/γ-Al_2O_3−I[c]	100	36.8	9.4	9.5	63.3
	200	35.7	10.6	9.4	62.8
	300	34.7	11.8	9.5	62.3
Fe−K/γ-Al_2O_3−II	100	39.0	8.1	8.1	67.1
	200	37.3	9.1	8.1	66.7
	300	36.3	10.1	8.1	66.3

[a]Experimental conditions: T = 300 °C, p = 10 bar, $GHSV_F$ = 1800 $mL_N\ h^{-1}\ g^{-1}$, $(H_2/CO_2)_{in}$ = 3, sieve fraction: 100−200 μm. [b]Based on gas phase analysis only, neglecting oxygenates ($S_{C_{5+},HC} = 1 - S_{C_1-C_4,HC}$). [c]Detailed results of this run have been previously published.[9]

The results indicate a slightly higher activity and higher selectivity to long-chain hydrocarbons for Fe−K/γ-Al_2O_3−II. We suspect that this is caused by the higher metal loading of Fe−K/γ-Al_2O_3−II. The metal loading of Fe−K/γ-Al_2O_3−I (prepared with an incipient wetness impregnation technique) could be well controlled and is close to the desired nominal loading (15 wt.-% Fe and 5.25 wt.-% K). The wet impregnation technique for Fe−K/γ-Al_2O_3−II, however, resulted in a higher metal loading which presumably increased the catalyst activity. Based on our global kinetic model for Fe−K/γ-Al_2O_3−I, the activity of Fe−K/γ-Al_2O_3−II is appr. 20% higher. Thus, we increased the catalyst mass by 20% within the simulations for

further comparison with experimental results whenever Fe−K/γ-Al_2O_3−II was used.

From a qualitative point of view, though, both catalysts behaved almost identically, and we did not observe a significant difference in the product composition. The long-term stability appeared to be similar: the average rate of activity decline (loss of abs.-% CO_2 conversion per day) was 0.2 and 0.3 for Fe−K/γ-Al_2O_3−I and Fe−K/γ-Al_2O_3−II, respectively. Thus, we considered it to be justified to apply the kinetic models developed for Fe−K/γ-Al_2O_3−I also for the experiments with Fe−K/γ-Al_2O_3−II.

4.1.2. Particle Size Variation. The results of the particle size variation tests with different sieve fractions of Fe−K/γ-Al_2O_3−II are given in Table 5. The CO_2 conversion was not affected by the variation of the particle size. Slight trends may be visible for H_2 and CO. For the CH_4 selectivity, however, an increase with particle size could be detected which went along with a slight decrease of the chain growth probability of short-chain hydrocarbons ($\alpha_{C_3-C_8}$).

Table 5. Results of the Particle Size Variation Tests[a]

sieve fraction (μm)	X_{CO_2}(%)	X_{H_2}(%)	S_{CO}(%)	$S_{CH_4/HC}$(%)	α_{C3-C8}(-)
50−100	30.0	23.6	32.2	9.4	0.72
100−200	29.8	23.3	32.2	9.9	0.72
300−400	29.1	22.8	34.3	11.9	0.70
500−1000	29.9	22.5	34.4	12.0	0.69

[a]Experimental conditions: T = 320 °C, p = 10 bar, $GHSV_F$ = 14 400 $mL_N\,h^{-1}\,g^{-1}$, $(H_2/CO_2)_{in}$ = 3, TOS = 50 h, catalyst: Fe−K/γ-Al_2O_3−II.

The results seem to indicate a slight intraparticle diffusional limitation for CO_2 and/or CO. The diffusivity of these species is significantly lower than for H_2 which can lead to higher H_2/CO_2 and H_2/CO ratios in the catalyst pores than in the gas bulk phase.[42] The results may have also been the consequence of a heat transfer limitation, though. To further investigate the combined transport effects of heat and mass, we performed 1D particle simulations that are provided in the Supporting Information.[43,44] Based on the simulations, external or internal heat transfer limitations are unlikely under the conditions applied. It is most likely that the observed effects are the result of a slight intraparticle diffusional limitation of CO_2 at the reactor entrance. This would, in turn, explain the slightly lighter product. However, since it did not yet significantly affect the reactant consumption, we neglected intraparticle diffusional limitation for further analysis of the experimental results via modeling. For even larger particles, it might become significant and may impose constraints on the catalyst design.

Intraparticle diffusional limitation was also reported by Kim et al. under similar conditions for extrudates of an Fe−K/γ-Al_2O catalyst with a diameter of ≤2.5 mm.[45] Unfortunately, we could not assess the originally prepared 1.5 mm extrudates under the exact same conditions without the risk of biasing the results with wall or distribution effects. The following recycle experiments were conducted with the particle size fraction 500−1000 μm which was most favorable from a practical point of view (low pressure drop, negligible wall effects, and simple handling).

4.2. Recycle Experiments. *4.2.1. Reactant Consumption.* One of the main motivations for recycle operation of CO_2-FTS with continuous product condensation is the increase of the overall reactant consumption. Water is the main product and strongly inhibits the reaction. Condensing the water and recycling the gas phase should thus be an effective way to increase the overall conversion.

The development of CO_2 conversion for the recycle experiments at $GHSV_F$ = 1800 $mL_N\,h^{-1}\,g^{-1}$ over TOS is shown in Figure 2. The beneficial influence of recycle operation on the overall CO_2 conversion can be clearly seen. Upon recycling product gas, the conversion could be significantly increased from ≈40% at R = 0 (once-through mode) to ≈60% at R = 1. The conversion per pass decreased upon increasing the recycle ratio. Please note that the fresh feed flow rate was kept constant during the experiments (see Section 2). So, the lower conversion per pass was mainly caused by the reduced residence time in the reactor per pass. Stable operation could be achieved up to R = 4 at an overall CO_2 conversion of ≈80%. When increasing R from 1 to 2 or 2 to 4, a relatively quick drop of the overall conversion could be observed which leveled off after a few hours. This was likely caused by the accumulation of hydrocarbons in the recycle loop which required several hours to reach steady state. Exemplary gas phase compositions are provided in the Supporting Information. At R = 8, we observed a pronounced and irreversible catalyst deactivation. The same was observed for the experiments at $GHSV_F$ = 3600 $mL_N\,h^{-1}\,g^{-1}$ at R = 8 and $GHSV_F$ = 7200 $mL_N\,h^{-1}\,g^{-1}$ at R = 4. Thus, this data was excluded from further analysis.

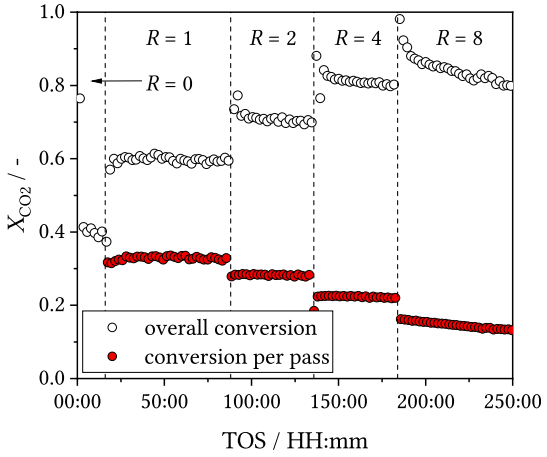

Figure 2. Development of CO_2 conversion (X_{CO_2}, overall and conversion per pass) with time-on-stream (TOS) for different recycle ratios (R); experimental conditions: T_W = 300 °C, p = 10 bar, $GHSV_F$ = 1800 $mL_N\,h^{-1}\,g^{-1}$, $(H_2/CO_2)_{in}$ = 3, R = 0−8, catalyst: Fe−K/γ-Al_2O_3−II (500−1000 μm).

We can only speculate about the reason for the deactivation as we have not specifically addressed this issue so far and cannot even exclude a technical issue associated with the setup at high recycle ratios that we are not aware of. Other authors have already investigated the deactivation behavior of Fe−K/γ-Al_2O_3 catalysts under once-through conditions, though. Carbonaceous deposits (carbon and/or coke) were reported by Hwang et al.[46] as a reason for the deactivation. Similarly, Lee et al.[47] reported coke from secondary reactions of alkenes as the main deactivation mechanism at the reactor outlet (along with phase transformation at the inlet). As the fraction of hydrocarbons (especially alkenes) significantly increases under recycle conditions (see Table S3), the coke deactivation

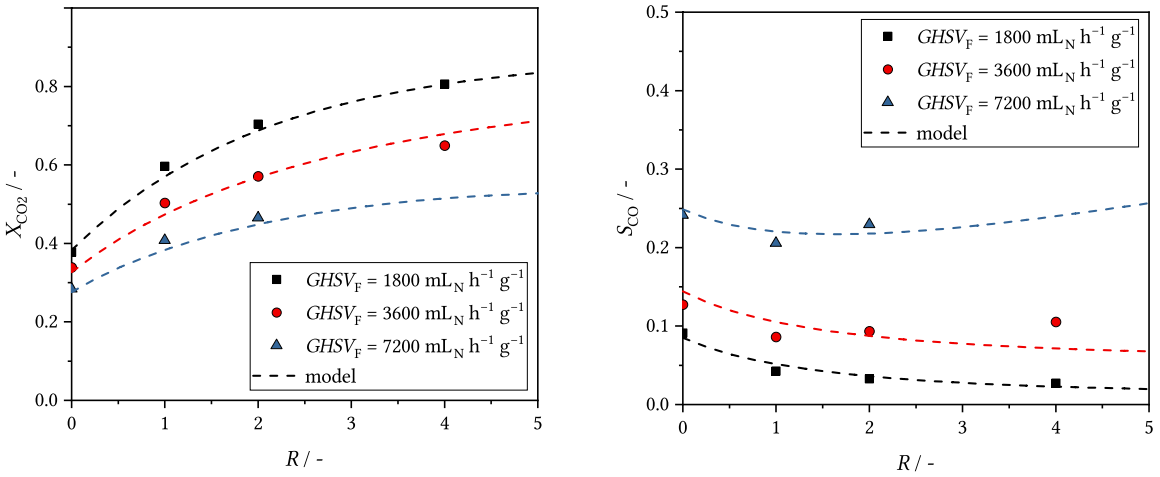

Figure 3. Overall conversion of CO_2 (X_{CO_2}, left) and selectivity to CO (S_{CO}, right) for different fresh feed space velocities and recycle ratios (R). Data points correspond to experimental values and dashed lines to simulation results. Experimental conditions: T_W = 300 °C, p = 10 bar, $GHSV_F$ = 1800−7200 $mL_N\,h^{-1}\,g^{-1}$, $(H_2/CO_2)_{in}$ = 3, R = 0−4, catalyst: Fe−K/γ-Al_2O_3−II (500−1000 μm). Deviating simulation conditions: T = 303 °C, 20% increased catalyst amount (see Section 3).

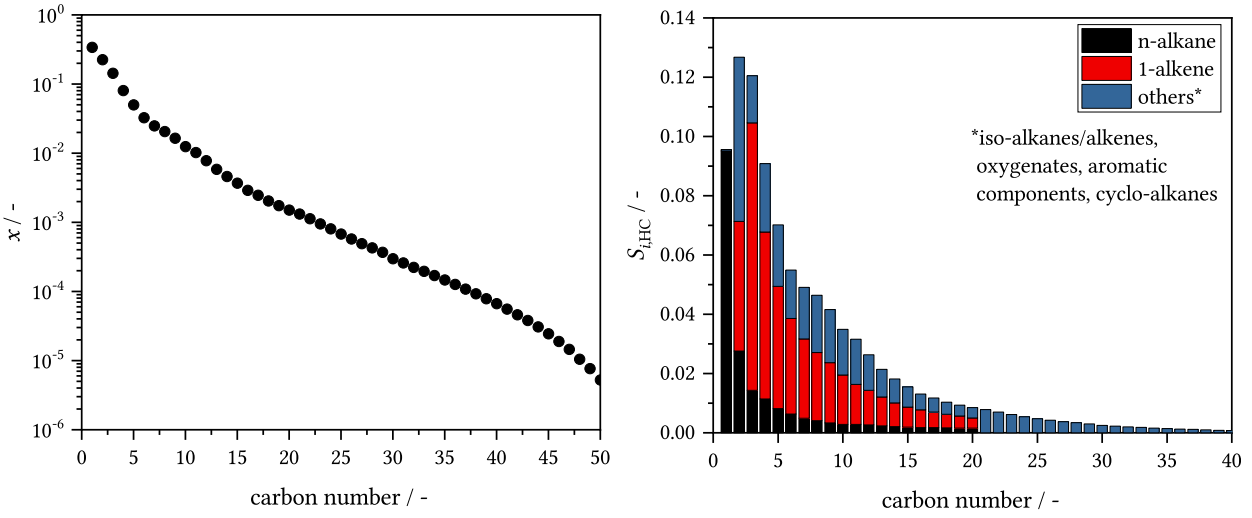

Figure 4. Mole fraction (x) vs carbon number (ASF plot, left) and hydrocarbon selectivity ($S_{i,HC}$) vs carbon number (right) for typical recycle conditions: X_{CO_2} = 70%, T_W = 300 °C, p = 10 bar, $GHSV_F$ = 1800 $mL_N\,h^{-1}\,g^{-1}$, $(H_2/CO_2)_{in}$ = 3, R = 2, catalyst: Fe−K/γ-Al_2O_3−II (500−1000 μm).

mechanism may be favored at high recycle ratios. For the experiments at $GHSV_F$ = 1800 $mL_N\,h^{-1}\,g^{-1}$ and R = 4, the molar fraction of hydrocarbons in the recycle gas amounted to almost 16%. In once-through mode, it did not even exceed 3% at the reactor outlet.

The extensive literature for the traditional iron-FTS may also be helpful for the interpretation. Carbon formation has always been a significant side reaction for the iron-based high-temperature Fischer−Tropsch process (HTFTS)[48] which has several similarities to the CO_2−FTS (see also section 4.2.2). Researchers at Sasol could link the rate of carbon formation to the ratio $p_{CO}/p_{H_2}^2$.[49] For the CO_2−FTS, this ratio varies significantly over the reactor length due to the consecutive reaction scheme of RWGS and FTS. On average, however, the ratio increases with an increasing recycle ratio (see Table S3) which may also partly explain the here observed deactivation behavior. Interestingly, operation at higher pressures reduces the rate of carbon formation for the HTFTS which is counterintuitive from a thermodynamic point of view.[49]

It is necessary to perform a more detailed study on the catalyst deactivation (with and without recycle) to understand its mechanism. This would help in finding suitable operational counter-measures and in improving the catalyst composition regarding long-term stability. From a technical point of view, we have to note, though, that recycle ratios > 3 may be considered unreasonably high. In section 4.2.2, it will also be shown that high recycle ratios are undesirable due to the influence of secondary reactions on the alkene selectivity.

The overall CO_2 conversion for all recycle experiments and the selectivity to CO in comparison to predictions of our detailed kinetic model are shown in Figure 3. An increase of the recycle ratio resulted in a higher conversion for all experiments. The model can reproduce the experimental trends and provides an estimate for the conversion with an error of less than 10%. For CO, however, there was no clear trend in the experiments. The CO selectivity decreased from R

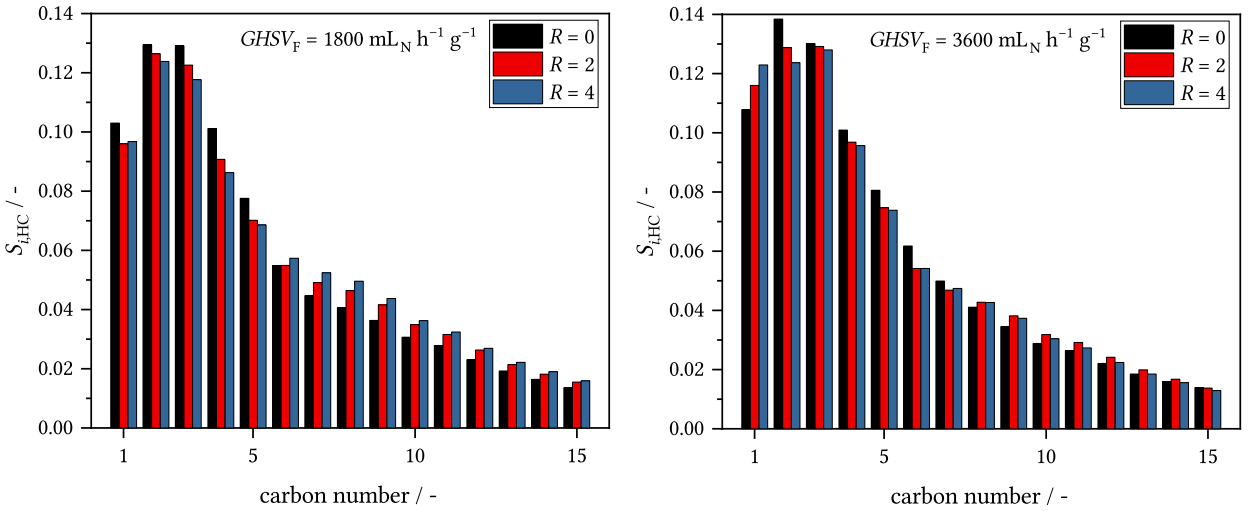

Figure 5. Hydrocarbon selectivity ($S_{i,HC}$) vs carbon number for different recycle ratios (R) and fresh feed space velocities ($GHSV_F$). Conditions: T_W = 300 °C, p = 10 bar, $GHSV_F$ = 1800 $mL_N\,h^{-1}\,g^{-1}$ (left), $GHSV_F$ = 1800 $mL_N\,h^{-1}\,g^{-1}$ (right), $(H_2/CO_2)_{in}$ = 3, catalyst: Fe−K/γ-Al_2O_3−II (500−1000 μm).

= 0 to R = 1 but then increased at higher recycle ratios for $GHSV_F$ = 3600 and 7200 $mL_N\,h^{-1}\,g^{-1}$. The prediction capability of the model for CO is worse than for CO_2 and may predict erroneous results for R > 2. It is interesting to note, though, that the model predicts an increase of S_{CO} at the highest $GHSV_F$ for high recycle ratios. This combination leads to low residence times in the reactor which are insufficient to convert CO that is initially formed via the RWGS. In that case, increasing the recycle ratio is expected to lead to a higher CO selectivity.

So, the developed model is capable of reproducing the trends in CO_2 conversion under recycle conditions and correctly accounts for the diluting effect of recycled hydrocarbons. The observed deactivation at high recycle ratios cannot be explained by the model, though.

4.2.2. Product Distribution. A typical product distribution of the CO_2-FTS under recycle conditions is shown in Figure 4 as an ASF and selectivity plot for an overall CO_2 conversion of 70%. The product spectrum mainly consists of short-chain hydrocarbons with a high fraction of 1-alkenes, very similar to the HTFTS.[50,51] Analogous to the HTFTS, Fe−K/γ-Al_2O_3−II displays a very pronounced selectivity to C_2 oxygenates (ethanol: 3.6%, ethanal: 0.7%, ethanoic acid: 1.2% for the conditions given in Figure 4). When these species are correctly considered, the often observed deviation for C_2 in the ASF plot[18,51] vanishes. This has also been reported for the HTFTS.[50] There is a noticeable dip in the distribution for the carbon range C_4−C_8. We suspect that this is an experimental artifact due to the evaporation of short-chain hydrocarbons from the oil phase (so-called *flash losses*). Gao et al.[52] demonstrated that this effect is especially relevant for the case of high conversions and low chain growth probabilities (which is the case here). Recycle operation further enhances this problem as the amount of condensed short-chain hydrocarbons increases.

Recycle operation has been suggested as an approach to increase the average chain length of the hydrocarbon products of CO_2-FTS[7,15,16] which may be desirable for fuel applications. So far though, no convincing experimental evidence could be provided for this theory. From a qualitative point of view, there are only small differences in comparison to the product distribution for the once-through mode that we had published previously.[9] Most notably, short-chain oxygenates could now be reliably measured. Besides that, the product seems to display a higher ethane/ethene ratio under recycle conditions. This topic will be addressed in more detail in Section 4.2.3. First, the influence of recycle operation on the overall carbon number distribution will be analyzed.

Figure 5 displays the carbon based selectivities to C_1−C_{15} species for different recycle ratios and fresh feed space velocities. The carbon number range 1−15 covers ≈85% of the hydrocarbon product and can thus be considered a representative excerpt of the whole product spectrum. Comparing ASF plots would be misleading, as the differences for short-chain products would be merely recognizable and the differences for very long chains (>C_{20}) would be strongly exaggerated (also due to a larger measurement uncertainty).

It can be seen that the hydrocarbon distribution was only slightly affected at different recycle ratios. Even at R = 4, no drastic changes could be detected. The data seems to support a slight increase of the average chain length (also observed for $GHSV_F$ = 7200 $mL_N\,h^{-1}\,g^{-1}$, not shown) under recycle conditions. Lee et al.[15] and Meiri et al.[7] have reported oligomerization of 1-alkenes as a possible mechanism. This theory will be discussed in more detail in the next section. We have to point out, though, that it is impossible to infer from the available data if the observed effect is due to secondary reactions of recycled hydrocarbons or due to a shift in the primarily formed product. Under recycle conditions, CO is already present at the very reactor inlet which may also explain the result. Either way, we conclude, at least for the conditions of this study, that recycle operation is not a reasonable measure to significantly increase the average chain length.

4.2.3. Secondary Reactions of 1-Alkenes. Before discussing the experimental results, it must be emphasized that, in principal, it is impossible to differentiate between secondary reactions of recycled products and a shift in the primarily formed products based on the obtained product spectrum. In a previous study, we investigated the change in product composition under once-through conditions for greatly varying residence times.[27] A slight change in the average chain length of the product could be observed for different residence times.

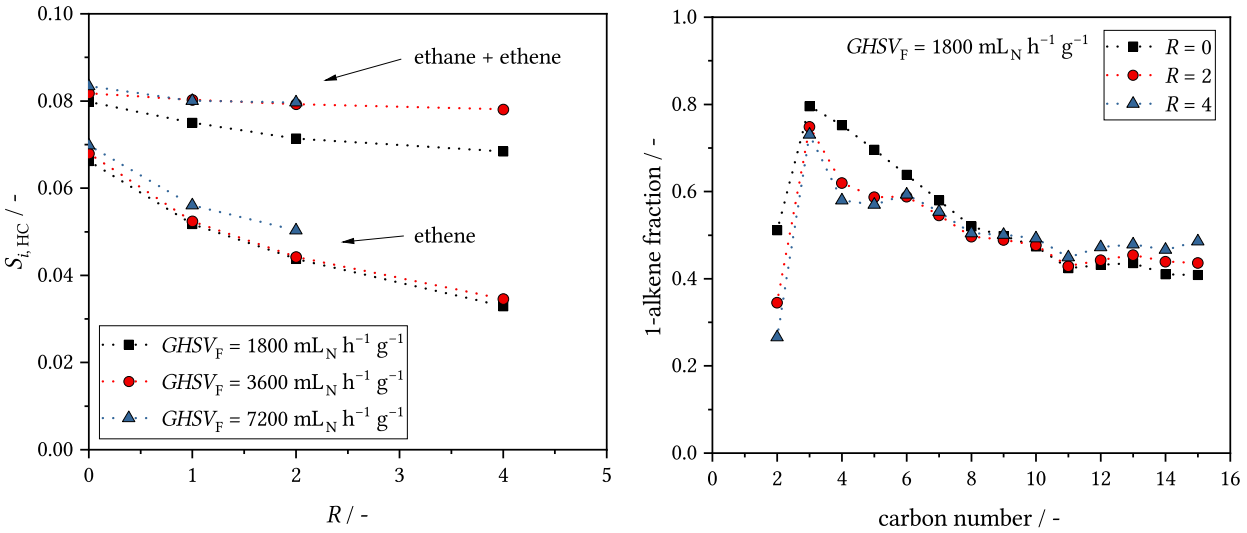

Figure 6. Development of ethene and ethane selectivities as a function of recycle ratio (R, left) and linear 1-alkene fraction within one carbon number for different R's at $GHSV_F$ = 1800 $mL_N\,h^{-1}\,g^{-1}$ (right). Dotted lines are only meant as a guidance. Conditions: T_W = 300 °C, p = 10 bar, $GHSV_F$ = 1800−7200 $mL_N\,h^{-1}\,g^{-1}$ (left), $GHSV_F$ = 1800 $mL_N\,h^{-1}\,g^{-1}$ (right), $(H_2/CO_2)_{in}$ = 3, catalyst: Fe−K/γ-Al_2O_3−II (500−1000 μm).

Table 6. Molar Fractions of C_4 Isomers within Gas Phase Analysis for Different Recycle Ratios and Fresh Feed Space Velocities

	$GHSV_F$ = 3600 $mL_N\,h^{-1}\,g^{-1}$				$GHSV_F$ = 1800 $mL_N\,h^{-1}\,g^{-1}$			
component	R = 0	R = 1	R = 2	R = 4	R = 0	R = 1	R = 2	R = 4
1-butene	78.9%	66.2%	62.3%	57.6%	79.2%	68.8%	66.6%	62.8%
n-butane	10.8%	13.1%	14.6%	16.9%	11.0%	12.8%	13.4%	14.5%
trans-2-butene	0.9%	6.4%	7.6%	8.9%	0.9%	5.1%	6.0%	7.3%
cis-2-butene	1.4%	6.1%	7.3%	8.6%	1.4%	4.9%	5.7%	7.0%
iso-butene	6.7%	6.9%	6.8%	6.7%	6.3%	6.9%	6.9%	6.9%
iso-butane	1.3%	1.3%	1.4%	1.4%	1.2%	1.4%	1.4%	1.5%

The composition within one carbon number, however, appeared to be relatively independent of the residence time. So, we have a high confidence that the results described below are actually due to secondary reactions of recycled 1-alkenes, except for the changes in chain length distribution.

When discussing secondary reactions of 1-alkenes for the traditional iron−FTS, the high reactivity of ethene is usually highlighted. Significant secondary hydrogenation has been reported in numerous studies.[19,20,24] The left graph in Figure 6 shows the development of the ethane + ethene and ethene selectivities for different recycle ratios and fresh feed space velocities. One can see that the selectivity to ethane + ethene remained almost constant or slightly decreased as a function of R. The selectivity to ethene, however, significantly decreased with increasing recycle ratio for all experiments. So, hydrogenation of ethene does also seem to be highly relevant under recycle conditions of CO_2−FTS. The data provided by Choi et al.[16] and Lee et al.[15] also supports this theory.

The right graph in Figure 6 shows the linear 1-alkene fraction within one carbon number for different recycle ratios for the experiments at $GHSV_F$ = 1800 $mL_N\,h^{-1}\,g^{-1}$. The fraction of linear 1-alkenes decreased up to C_8 under recycle conditions and even seemed to slightly increase for higher carbon numbers. The intersection of the dotted lines corresponds well with the phase split between oil and gas phase (see the Supporting Information). Hydrocarbons up to C_8 were partly recycled and could undergo further reactions (such as hydrogenation), while longer-chained products were removed from the gas loop through condensation.

Additionally to ethene, there was also a remarkable drop for the fractions of 1-butene and 1-pentene. A detailed analysis is challenging as C_4 and C_5 species were partially condensed, and we could not clearly differentiate between all isomers. However, it was still possible to analyze the relative amounts of C_4 isomers in the gas phase analysis (excluding oxygenates). It is unlikely that the distribution of isomers was significantly distorted by their slightly different volatilities.

The molar fractions of C_4 isomers within the gas phase analysis are given in Table 6 for different recycle ratios at $GHSV_F$ = 1800 and 3600 $mL_N\,h^{-1}\,g^{-1}$. A decrease of the 1-butene fraction with increasing recycle ratio can be clearly seen (≈80% at R = 0 versus ≈60% at R = 4). Some of the 1-butene seemed to be hydrogenated to *n*-butane. The majority, however, seemed to undergo a double-bond-shift to trans-2-butene and cis-2-butene. 2-Butenes were almost absent in the primary product (≈ 1% each at R = 0). For $GHSV_F$ = 3600 $mL_N\,h^{-1}\,g^{-1}$, the fractions increased to almost ≈9% each at R = 4. There seemed to be a slight preference for cis-2-butene in the primarily formed product but a slight preference for trans-2-butene at increased recycling. There was no sign for skeletal isomerization as the fractions of iso-butane and iso-butene remained constant. Double-bond-shift could also be qualitatively observed in the oil phase chromatograms for C_5−C_8. Hanlon et al.[21] reported the same experimental trends for 1-

butene cofeeding experiments under traditional iron−FTS conditions at low CO partial pressures.

The possibility of secondary growth of 1-alkenes is more difficult to assess from the available data. Lee et al.[15] and Meiri et al.[7] have reported oligomerization of 1-alkenes to be responsible for an increase of the average chain length under recycle conditions or for multiple reactors in series. Presumably, the authors are referring to 1-alkene reincorporation/secondary growth which can result in an increase of the average chain length and may also be considered as some type of oligomerization reaction. Heterogeneously catalyzed oligomerization of alkenes is actually performed on strongly acidic catalysts[51] which is not the case here as CO_2−FTS catalysts are usually alkali promoted.[4,5,53] CO_2−FTS-catalysts may be mixed with a strongly acidic catalyst (e.g., H-ZSM5[54]). That is a completely different case, though, which is explicitly not considered here.

Incorporation of ethene into longer chains has been clearly demonstrated for the traditional iron−FTS (even for HTFTS) in ^{14}C tracer cofeeding studies.[19,22,23] It did not amount to more than 10% of the converted tracer, though. Hydrogenation to ethane was the dominant reaction under all conditions. So, in principle, it seems to be chemically possible that an increase of the average chain length is caused by secondary reactions of recycled 1-alkenes. However, the effect would likely be only minor. As stated in the previous section, the observed slight increase in average chain length may have also been the result of a more beneficial H_2/CO ratio which led to a shift in the primarily formed product.

Hydrogenolysis and carbonylation of ethene have also been observed for traditional iron−FTS conditions to a small extent[19,22] in ^{14}C tracer cofeeding studies. Our data does not indicate a significant contribution of either of these reactions, though.

5. CONCLUSION AND OUTLOOK

The main motivation for recycle operation of the catalytic hydrogenation of CO_2 to long-chain hydrocarbons (CO_2−FTS) is the increase of reactant conversion. As the reaction is strongly inhibited by the main product, water, the continuous removal of condensable products and recirculation of unconverted gas is an obvious approach. The validity of the concept could be clearly demonstrated here in a bench scale recycle reactor setup, and a stable CO_2 conversion of up to 80% at $R = 4$ and $GHSV_F = 1800\ mL_N\ h^{-1}\ g^{-1}$ could be achieved with a potassium promoted, alumina supported iron catalyst. When aiming for the operation of the reaction in multitubular fixed bed reactors, recycle operation is also beneficial from an operational point of view. Under recycle conditions, more uniform reaction conditions along the catalyst bed can be achieved. Additionally, this leads to increased gas velocities which improve the heat removal. This can simplify the thermal design of the reactor or allow for operation under more severe conditions.[55]

Catalyst deactivation is a challenging topic for the further development of CO_2−FTS. Our data indicates an increased deactivation under recycle conditions. It is highly desirable to perform a more detailed study to understand the underlying mechanisms (with and without recycle) and find suitable countermeasures. One approach may be the application of a reactor concept that allows for continuous catalyst replacement and external regeneration, e.g. a fluidized bed reactor.

The observed secondary reactions agree well with reported results for the traditional FTS on iron based catalysts, with ethene hydrogenation being the most prevalent reaction. Based on the isomer distribution of gas-phase C_4 species, hydrogenation and double-bond-shift of linear, long-chain 1-alkenes could also be verified. For a more detailed understanding of the secondary reaction pathways, it is necessary to perform cofeeding experiments, ideally with small amounts of radioactively labeled 1-alkenes. Recycle operation did not result in a significant increase of the average chain length. So, from our point of view, it is a rather poor approach to achieve a higher molecular weight product. Operation at high recycle ratios mainly leads to a loss of primarily formed, high value 1-alkenes which is highly undesirable. For fuel applications, e.g. the production of sustainable jet fuel or diesel, it appears more reasonable to refine the primarily formed 1-alkenes to middle distillates with an appropriate oligomerization technology.[51]

AUTHOR INFORMATION

Corresponding Author

Lucas Brübach − *Institute for Micro Process Engineering (IMVT), Karlsruhe Institute of Technology (KIT), 76344 Eggenstein-Leopoldshafen, Germany;* orcid.org/0000-0002-9530-8256; Phone: +49 (0)721 608-24094; Email: lucas.bruebach@kit.edu

Authors

Dennis Trützler − *Institute for Micro Process Engineering (IMVT), Karlsruhe Institute of Technology (KIT), 76344 Eggenstein-Leopoldshafen, Germany*

Daniel Hodonj − *Institute for Micro Process Engineering (IMVT), Karlsruhe Institute of Technology (KIT), 76344 Eggenstein-Leopoldshafen, Germany*

Peter Pfeifer − *Institute for Micro Process Engineering (IMVT), Karlsruhe Institute of Technology (KIT), 76344 Eggenstein-Leopoldshafen, Germany*

Notes

The authors declare no competing financial interest.

ACKNOWLEDGMENTS

This work was funded by the German Federal Ministry for Economic Affairs and Climate Action (BMWK) under the project acronym PowerFuel, funding number 03EIV071B. The authors thank Malina Burcea (CVT, KIT) for the N_2 physisorption and Hg porosimetry measurements, and Dr. Thomas Bergfeldt (IAM-AWP, KIT) for the ICP-OES analyses.

NOMENCLATURE

Symbols

α = chain growth probability

Bo = Bodenstein number
d_P = particle diameter (m)
d_T = reactor diameter (here: width of annulus between outer wall and central tube, m)
$GHSV_F$ = fresh feed gas hourly space velocity ($mL_N\,h^{-1}\,g^{-1}$)
m = mass (kg)
$\dot{m}$ = mass flow rate ($kg\,s^{-1}$)
$n_{i,C}$ = number of carbon atoms in component i
$\dot{n}_i$ = molar flow rate of component i ($mol\,h^{-1}$)
p = pressure (bar)
R = recycle ratio (weight based)
S_{CO} = CO selectivity
$S_{i,HC}$ = carbon based, CO-free, selectivity to hydrocarbon i
T = temperature (°C/K)
T_W = outer reactor wall temperature (°C/K)
V_N = volumetric flow rate at normal conditions (0 °C and 1 atm, $mL_N\,min^{-1}$)
x = mole fraction
X_i = conversion of component i

Subscripts and Superscripts

cat = catalyst
F = fresh feed
i,j = species i/j
in = system inlet
N = normal conditions (0 °C and 1 atm)
out = system outlet
R = recycle

Abbreviations

ASF = Anderson−Schulz−Flory
BET = Brunauer−Emmet−Teller
BPR = back pressure regulator
FIC = flow indicator controller
FID = flame ionization detector
FT = Fischer−Tropsch
FTS = Fischer−Tropsch synthesis
GC = gas chromatograph
HTFTS = high-temperature Fischer−Tropsch synthesis
ICP-OES = inductively coupled plasma optical emission spectrometry
ID = inner diameter
OD = outer diameter
MFC = mass flow controller
PFR = plug flow reactor
PI = pressure indicator
PR = pressure regulator
RWGS = reverse water gas shift
TCD = thermal conductivity detector
TI = temperature indicator
TIC = temperature indicator controller
TOS = time-on-stream
VLE = vapor−liquid equilibrium
VLLE = vapor−liquid−liquid equilibrium

REFERENCES

(1) Atsbha, T. A.; Yoon, T.; Seongho, P.; Lee, C.-J. A review on the catalytic conversion of CO2 using H2 for synthesis of CO, methanol, and hydrocarbons. *J. CO2 Util.* **2021**, *44*, 101413.
(2) Ra, E. C.; Kim, K. Y.; Kim, E. H.; Lee, H.; An, K.; Lee, J. S. Recycling Carbon Dioxide through Catalytic Hydrogenation: Recent Key Developments and Perspectives. *ACS Catal.* **2020**, *10*, 11318−11345.
(3) Gao, P.; Zhang, L.; Li, S.; Zhou, Z.; Sun, Y. Novel Heterogeneous Catalysts for CO2 Hydrogenation to Liquid Fuels. *ACS Cent. Sci.* **2020**, *6*, 1657−1670.
(4) Panzone, C.; Philippe, R.; Chappaz, A.; Fongarland, P.; Bengaouer, A. Power-to-Liquid catalytic CO2 valorization into fuels and chemicals: focus on the Fischer−Tropsch route. *J. CO2 Util.* **2020**, *38*, 314−347.
(5) Wei, J.; Yao, R.; Han, Y.; Ge, Q.; Sun, J. Towards the development of the emerging process of CO2 heterogenous hydrogenation into high-value unsaturated heavy hydrocarbons. *Chem. Soc. Rev.* **2021**, *50*, 10764−10805.
(6) Ye, R.-P.; Ding, J.; Gong, W.; Argyle, M. D.; Zhong, Q.; Wang, Y.; Russell, C. K.; Xu, Z.; Russell, A. G.; Li, Q.; Fan, M.; Yao, Y.-G. CO2 hydrogenation to high-value products via heterogeneous catalysis. *Nat. Commun.* **2019**, *10*, 5698.
(7) Meiri, N.; Radus, R.; Herskowitz, M. Simulation of novel process of CO2 conversion to liquid fuels. *J. CO2 Util.* **2017**, *17*, 284−289.
(8) Landau, M. V.; Vidruk, R.; Herskowitz, M. Sustainable production of green feed from carbon dioxide and hydrogen. *ChemSusChem* **2014**, *7*, 785−794.
(9) Brübach, L.; Hodonj, D.; Pfeifer, P. Kinetic Analysis of CO2 Hydrogenation to Long-Chain Hydrocarbons on a Supported Iron Catalyst. *Ind. Eng. Chem. Res.* **2022**, *61*, 1644−1654.
(10) Iglesias, G. M.; de Vries, C.; Claeys, M.; Schaub, G. Chemical energy storage in gaseous hydrocarbons via iron Fischer−Tropsch synthesis from H2/CO2—Kinetics, selectivity and process considerations. *Catal. Today* **2015**, *242*, 184−192.
(11) Rohde, M. P.; Unruh, D.; Schaub, G. Membrane Application in Fischer−Tropsch Synthesis to Enhance CO2 Hydrogenation. *Ind. Eng. Chem. Res.* **2005**, *44*, 9653−9658.
(12) Li, Z.; Deng, Y.; Dewangan, N.; Hu, J.; Wang, Z.; Tan, X.; Liu, S.; Kawi, S. High Temperature Water Permeable Membrane Reactors for CO2 Utilization. *Chem. Eng. J.* **2021**, *420*, 129834.
(13) Kölbel, H.; Ackermann, P.Process for catalytic reduction of carbon dioxide with hydrogen. U.S. Patent 2,692,274. 1954.
(14) Guo, L.; Cui, Y.; Zhang, P.; Peng, X.; Yoneyama, Y.; Yang, G.; Tsubaki, N. Enhanced Liquid Fuel Production from CO2 Hydrogenation: Catalytic Performance of Bimetallic Catalysts over a Two-Stage Reactor System. *ChemistrySelect* **2018**, *3*, 13705−13711.
(15) Lee, S.-B.; Kim, J.-S.; Lee, W.-Y.; Lee, K.-W.; Choi, M.-J. In *Carbon dioxide utilization for global sustainability*; Park, S.-E., Chang, J.-S., Lee, K.-W., Eds.; Studies in surface science and catalysis; Elsevier: 2004; Vol. *153*, pp 73−78, DOI: 10.1016/S0167-2991(04)80222-2.
(16) Choi, M. J.; Kim, J.; Lee, S.; Lee, W.; Lee, K. In *Greenhouse gas control technologies*; Gale, J., Kaya, Y., Eds.; Pergamon: Amsterdam and Oxford, 2003; Vol. *II*, pp 1491−1496.
(17) Willauer, H. D.; Bradley, M. J.; Baldwin, J. W.; Hartvigsen, J. J.; Frost, L.; Morse, J. R.; DiMascio, F.; Hardy, D. R.; Hasler, D. J. Evaluation of CO2 Hydrogenation in a Modular Fixed-Bed Reactor Prototype. *Catalysts* **2020**, *10*, 970.
(18) Chakrabarti, D.; Prasad, V.; de Klerk, A. In *Fischer−Tropsch Synthesis, Catalysts, and Catalysis*; Davis, B. H., Occelli, M. L., Eds.; Chemical industries; CRC Press: Bosa Roca, 2016; Vol. *118*, pp 183−222.
(19) Schulz, H.; Rao, B. R.; Elstner, M. 14C-Studien zum Reaktionmechanismus der Fischer−Tropsch-Synthese. *Erdoel, Kohle, Erdgas, Petrochem* **1970**, *23*, 651−655.
(20) Botes, F. G.; Govender, N. S. Secondary Reactions of Ethylene As Studied in a Laboratory-Scale Recycle Slurry Reactor. *Energy Fuels* **2007**, *21*, 3095−3101.
(21) Hanlon, R. T.; Satterfield, C. N. Reactions of selected 1-olefins and ethanol added during the Fischer−Tropsch synthesis. *Energy Fuels* **1988**, *2*, 196−204.
(22) Tau, L. M.; Dabbagh, H. A.; Davis, B. H. Fischer−Tropsch synthesis: carbon-14 tracer study of alkene incorporation. *Energy Fuels* **1990**, *4*, 94−99.

(23) Pichler, H.; Schulz, H. Neuere Erkenntnisse auf dem Gebiet der Synthese von Kohlenwasserstoffen aus CO und H2. *Chemie Ing. Techn.* **1970**, *42*, 1162−1174.
(24) Boelee, J. H.; Cüsters, J.; van der Wiele, K. Influence of reaction conditions on the effect of Co-feeding ethene in the Fischer−Tropsch synthesis on a fused-iron catalyst in the liquid phase. *Applied Catalysis* **1989**, *53*, 1−13.
(25) König, L.; Gaube, J. Fischer−Tropsch-Synthese. Neuere Untersuchungen und Entwicklungen. *Chem. Ing. Technol.* **1983**, *55*, 14−22.
(26) Landau, M. V.; Meiri, N.; Utsis, N.; Vidruk Nehemya, R.; Herskowitz, M. Conversion of CO2, CO, and H2 in CO2 Hydrogenation to Fungible Liquid Fuels on Fe-Based Catalysts. *Ind. Eng. Chem. Res.* **2017**, *56*, 13334−13355.
(27) Brübach, L.; Hodonj, D.; Biffar, L.; Pfeifer, P. Detailed Kinetic Modeling of CO2-Based Fischer−Tropsch Synthesis. *Catalysts* **2022**, *12*, 630.
(28) Holderbaum, T.; Gmehling, J. PSRK: A Group Contribution Equation of State Based on UNIFAC. *Fluid Phase Equilib.* **1991**, *70*, 251−265.
(29) Gmehling, J. Present status and potential of group contribution methods for process development. *J. Chem. Thermodyn.* **2009**, *41*, 731−747.
(30) Gmehling, J.; Kolbe, B.; Kleiber, M.; Rarey, J. R.*Chemical thermodynamics for process simulation*; Wiley-VCH-Verl.: Weinheim, 2012.
(31) Soave, G. Equilibrium constants from a modified Redlich-Kwong equation of state. *Chem. Eng. Sci.* **1972**, *27*, 1197−1203.
(32) Fredenslund, A.; Jones, R. L.; Prausnitz, J. M. Group-contribution estimation of activity coefficients in nonideal liquid mixtures. *AIChE J.* **1975**, *21*, 1086−1099.
(33) Ahlers, J.; Gmehling, J. Development of an universal group contribution equation of state: I. Prediction of liquid densities for pure compounds with a volume translated Peng−Robinson equation of state. *Fluid Phase Equilib.* **2001**, *191*, 177−188.
(34) Fischer, K.; Gmehling, J. Further development, status and results of the PSRK method for the prediction of vapor-liquid equilibria and gas solubilities. *Fluid Phase Equilib.* **1996**, *121*, 185−206.
(35) Li, J.; Fischer, K.; Gmehling, J. Prediction of vapor−liquid equilibria for asymmetric systems at low and high pressures with the PSRK model. *Fluid Phase Equilib.* **1998**, *143*, 71−82.
(36) Rachford, H. H., Jr.; Rice, J. D. Procedure for Use of Electronic Digital Computers in Calculating Flash Vaporization Hydrocarbon Equilibrium. *J. Pet. Technol.* **1952**, *4*, 19.
(37) Peng, D.-Y.; Robinson, D. B. Two and three phase equilibrium calculations for systems containing water. *Can. J. Chem. Eng.* **1976**, *54*, 595−599.
(38) Turek, E. A.; Metcalfs, R. S.; Yarborough, L.; Robinson, R. L., Jr. Phase Equilibria in CO2 - Multicomponent Hydrocarbon Systems: Experimental Data and an Improved Prediction Technique. *SPEJ, Soc. Pet. Eng. J.* **1984**, *24*, 308−324.
(39) Huang, S. H.; Lin, H. M.; Tsai, F. N.; Chao, K. C. Solubility of synthesis gases in heavy n-paraffins and Fischer−Tropsch wax. *Ind. Eng. Chem. Res.* **1988**, *27*, 162−169.
(40) Huang, S. H.; Lin, H. M.; Chao, K. C. Solubility of carbon dioxide, methane, and ethane in n-octacosane. *J. Chem. Eng. Data* **1988**, *33*, 143−145.
(41) Mathias, P. M.; Copeman, T. W. Extension of the Peng-Robinson equation of state to complex mixtures: Evaluation of the various forms of the local composition concept. *Fluid Phase Equilib.* **1983**, *13*, 91−108.
(42) Vervloet, D.; Kapteijn, F.; Nijenhuis, J.; van Ommen, J. R. Fischer−Tropsch reaction−diffusion in a cobalt catalyst particle: aspects of activity and selectivity for a variable chain growth probability. *Catal. Sci. Technol.* **2012**, *2*, 1221−1233.
(43) Solsvik, J.; Jakobsen, H. A. Modeling of multicomponent mass diffusion in porous spherical pellets: Application to steam methane reforming and methanol synthesis. *Chem. Eng. Sci.* **2011**, *66*, 1986−2000.
(44) Güttel, R.; Turek, T.*Chemische Reaktionstechnik*, 1st ed.; Springer: Berlin, Heidelberg, 2021; DOI: 10.1007/978-3-662-63150-8.
(45) Kim, J.-S.; Lee, S.; Lee, S.-B.; Choi, M.-J.; Lee, K.-W. Performance of catalytic reactors for the hydrogenation of CO2 to hydrocarbons. *Catal. Today* **2006**, *115*, 228−234.
(46) Hwang, J. S.; Jun, K.-W.; Lee, K.-W. Deactivation and regeneration of Fe-K/alumina catalyst in CO2 hydrogenation. *Appl. Catal., A* **2001**, *208*, 217−222.
(47) Lee, S.-C.; Kim, J.-S.; Shin, W. C.; Choi, M.-J.; Choung, S.-J. Catalyst deactivation during hydrogenation of carbon dioxide: Effect of catalyst position in the packed bed reactor. *J. Mol. Catal. A: Chem.* **2009**, *301*, 98−105.
(48) Dry, M. E. In *Catalysis*; Anderson, J. R., Boudart, M., Eds.; Springer: Berlin, 1981; pp 159−255.
(49) Dry, M. E. Predict Carbonation Rate on Iron Catalyst. *Hydrocarb. Process.* **1980**, *59*, 92−94.
(50) Weitkamp, A. W.; Frye, C. G. Products of Hydrogenation of Carbon Monoxide - Relation of Product Composition to Reaction Mechanism. *Ind. Eng. Chem. Res.* **1953**, *45*, 363−367.
(51) de Klerk, A.*Fischer−Tropsch refining*, 1st ed.; Wiley-VCH: Weinheim, 2011; DOI: 10.1002/9783527635603.
(52) Gao, J.; Wu, B.; Zhou, L.; Yang, Y.; Hao, X.; Xu, J.; Xu, Y.; Li, Y. Irregularities in Product Distribution of Fischer−Tropsch Synthesis Due to Experimental Artifact. *Ind. Eng. Chem. Res.* **2012**, *51*, 11618−11628.
(53) Wang, D.; Xie, Z.; Porosoff, M. D.; Chen, J. G. Recent advances in carbon dioxide hydrogenation to produce olefins and aromatics. *Chem.* **2021**, *7*, 2277−2311.
(54) Wei, J.; Ge, Q.; Yao, R.; Wen, Z.; Fang, C.; Guo, L.; Xu, H.; Sun, J. Directly converting CO2 into a gasoline fuel. *Nat. Commun.* **2017**, *8*, 15174.
(55) Sie, S. T.; Krishna, R. Fundamentals and selection of advanced Fischer−Tropsch reactors. *Appl. Catal., A* **1999**, *186*, 55−70.